Melt-Intercalation Nanocomposites with Fluorinated Polymers and a Correlation for Nanocomposite Formation

Younghoon Kim, James L. White

Institute of Polymer Engineering, University of Akron, Akron, Ohio 44325

Received 1 April 2003; accepted 2 September 2003

ABSTRACT: Various fluorinated polymers were investigated to produce polymer nanocomposites with special clays. Natural and organically treated montmorillonite clays were melt-compounded with the polymers. Characterization by wide-angle X-ray scattering and transmission electron microscopy showed the separation of montmorillonite layers and the formation of polymer nanocomposites. Organically treated montmorillonite clay dispersed in poly(vinylidene fluoride) and various vinylidene fluoride copolymers and formed nanocomposites. Natural and organophilic clays were not well dispersed in other fluorinated copolymers and polyethylene. A correlation was developed for the formation of polymer–clay nanocomposite structures in chlorinated and fluorinated polymers in terms of the dielectric constant. © 2004 Wiley Periodicals, Inc. J Appl Polym Sci 92: 1061–1071, 2004

Key words: nanocomposites; clay; fluoropolymers; compounding; dielectric properties

INTRODUCTION

Since the synthesis of poly(tetrafluoroethylene) in 1938, fluoropolymers have been developed for high-performance industrial applications.[1–3] In the 1950s, poly(vinylidene fluoride) (PVDF) and various copolymers with hexafluoropropylene and tetrafluoroethylene were developed. Fluoropolymers are noted for their excellent resistance against chemicals, weathering, and high temperatures.

In this article, we are concerned with the characteristics of compounds of fluoropolymers with montmorillonite (MMT) clay. There is a long history of investigations of intersilicate sheet swelling of clays by polar organic liquids.[4–9] The clays primarily studied so far are MMTs. In the 1980s, the *in situ* polymerization of ϵ-caprolactam with MMT clay to produce polymer nanocomposites was developed by the Toyota Research Center. The Toyota laboratory succeeded in producing polyamide-6 nanocomposites by polymerizing ϵ-caprolactam that contained swollen MMT. Polyamide-6/clay nanocomposites at low clay levels unexpectedly had higher tensile moduli and strength than pure polyamide 6.[10–16] They licensed this invention to Ube Kosan, which commercialized nylon–clay hybrids based on polyamide 6. The films had high levels of barrier properties.

Many polymer nanocomposites are made from thermoplastics by melt blending. These include polyamide 66,[17] poly(ethylene-*co*-vinyl acetate),[18] and poly(vinyl chloride) (PVC).[19,20] These polymers are generally polar. In a previous study, we succeeded in making polymer–clay nanocomposites with various chlorinated polymers, including chlorinated polyethylene (PE), polychloroprene (CR), PVC, chlorinated PVC, and poly(vinylidene chloride) (PVDC), and we showed enhanced mechanical properties for chlorinated polymer nanocomposites.[21] This was found not to be possible with nonpolar PE or polypropylene (PP). However, other authors[22–27] have found it possible to produce nanocomposites from these polymers by grafting maleic anhydride onto them.

There have been few investigations of fluoropolymer nanocomposites. Melt-intercalated PVDF–clay nanocomposites were recently described by Priya and Jog.[28] Recent patents[29,30] have involved efforts to produce nanocomposites from fluoroelastomers and amorphous fluoropolymers. In this article, we describe an investigation of nanocomposites forming from various fluorinated polymers. We also develop a correlation for the formation of nanocomposites by melt intercalation based on the polymeric structure.

EXPERIMENTAL

Materials

A wide range of fluorinated polymers were investigated in this study; they are summarized in Table I. They include, in order of their fluorine contents, PE, PVDF, poly(vinylidene fluoride-tetrafluoroethylene-perfluoromethyl vinyl ether-cure site monomer) [P(VDF-TFE-MVE-CSM)], poly(vinylidene fluoride-hexafluoropro-

Correspondence to: J. L. White.

Journal of Applied Polymer Science, Vol. 92, 1061–1071 (2004)

TABLE I
Polymers

Material	Fluorine content (wt %)	Commercial name	T_m (°C)	T_g (°C)	Supplier
PE	0	2045 LLDPE	122	—	Dow Chemical
P(E-CTFE)	37.5	Vatar	180	—	Ausimont
PVDF	58	Solef 1008	173	−32	Solvay
P(VDF-TFE-MVE-CSM)	64	Viton GLT	—	~−30	DuPont Dow Elastomers
P(VDF-HFP)	66	Viton A 200	—	−18	DuPont Dow Elastomers
P(VDF-HFP-TFE)	68.5	Viton B 600	—	−13	DuPont Dow Elastomers
P(TFE-HFP)	75	Teflon FEP	264	—	DuPont

T_m = melting temperature; T_g = glass-transition temperature.

pylene) [P(VDF-HFP)], poly(vinylidene fluoride-hexafluoropropylene-tetrafluoroethylene) [P(VDF-HFP-TFE)], poly(tetrafluoroethylene-hexafluoropropylene) [P(TFE-HFP)], and poly(ethylene-chlorotrifluoroethylene) [P(E-CTFE)]. The latter polymer has the structural unit —(CH_2—CH_2)—(CFCl—CF_2)—.

Southern Clay Co. supplied MMT clays (Cloisite Na^+ and Cloisite 20A). Cloisite Na^+ is a natural MMT. Cloisite 20A is an organically treated MMT with dimethyl dihydrogenated tallow quaternary ammonium.

Compounding

Compounding was carried out in a Brabender internal mixer. PE, P(E-CTFE), and PVDF were compounded at 180°C at a rotor speed of 100 rpm. Mixing was carried out for 5 min. The polymers and clay (wt %) were premixed in a beaker. All the fluoroelastomers were compounded at 90°C and 50 rpm.

Characterization

A Bruker X-ray machine with a wavelength of λ = 1.5422 Å was used. Powder diffraction patterns were prepared for P(TFE-HFP), PVDF, P(E-CTFE), and PE. Fluoroelastomers were sliced into thin specimens for X-ray diffraction (XRD).

A Tecnai-12 transmission electron microscope operated at 120 kV was used to take images of the specimens. Ultrathin sectioning was performed with a Reichert Ultracut sectioning system.

Dog-bone-shaped specimens were prepared by compression molding for tensile testing in an Instron tensile machine. The ASTM D 638 method was used. No mechanical testing was performed for fluoroelastomers because of the shrinkage of the molded specimens if they were not vulcanized. Vulcanization during molding introduced another variable that we did not wish to treat at this time.

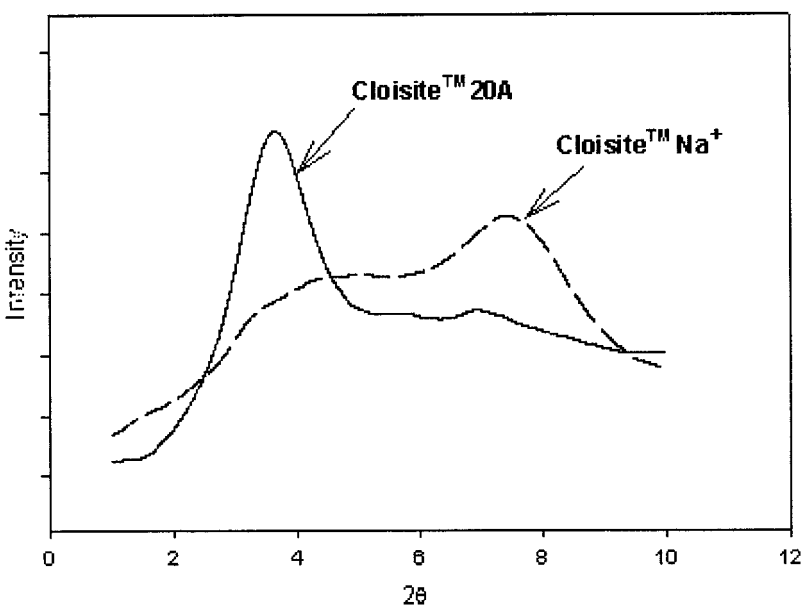

Figure 1 XRD patterns of Cloisite 20A and Na^+ MMT clays.

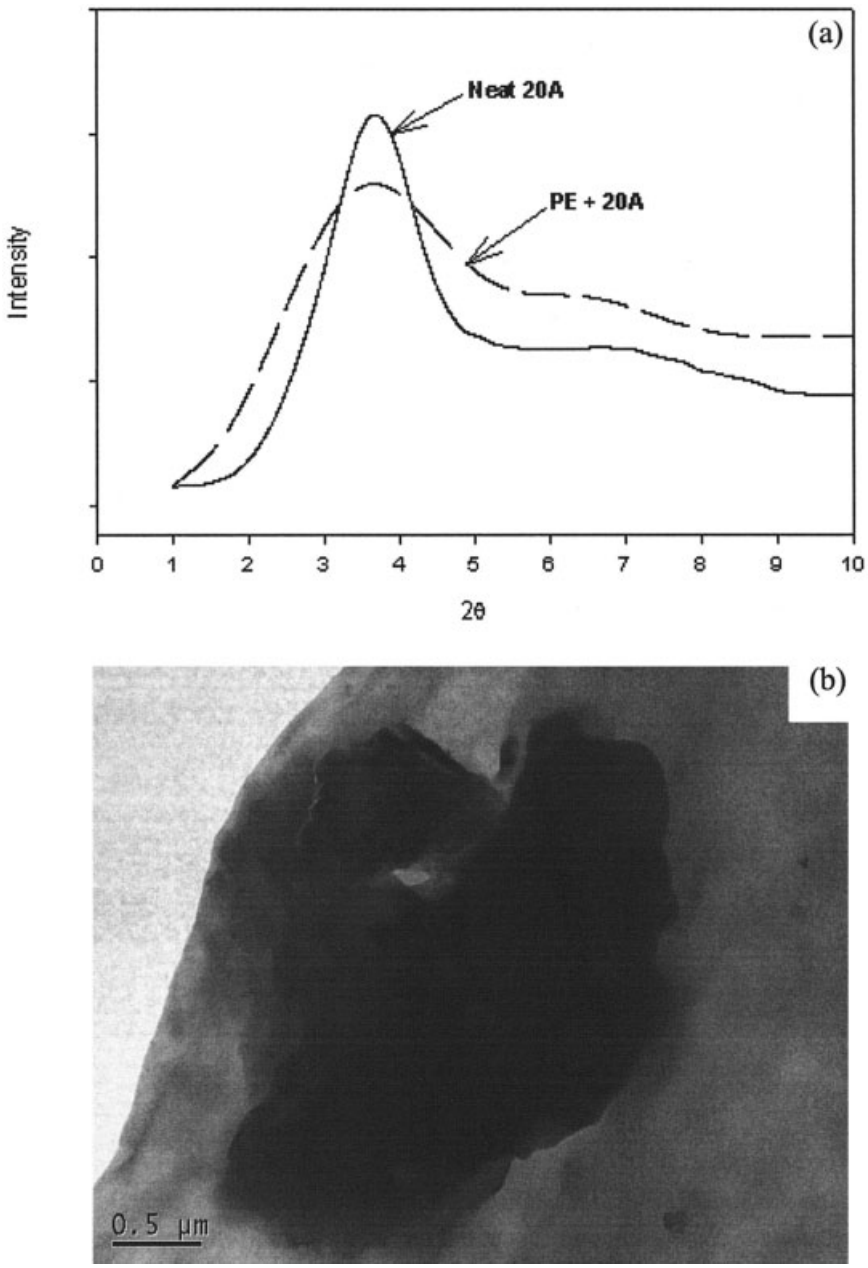

Figure 2 (a) XRD patterns of PE/20A and (b) TEM image of a P(E-CTFE)/20A compound.

RESULTS

Here we present our results. We first consider XRD of the clays and then wide-angle X-ray scattering (WAXS) and transmission electron microscopy (TEM) studies of the clay-modified polymers. We present our results in order of the weight percentage of fluorine.

Clay

Cloisite Na^+ (natural MMT) was observed to have a strong *d*-spacing of 11.7 Å at $2\theta = 7.55°$ (Fig. 1). This is well known[4] to represent the distance between silicate layers. The organically treated MMT Cloisite 20A clay exhibited a *d*-spacing peak at $2\theta = 3.65°$, which represents a *d*-spacing of 24.2 Å. Other representative crystalline peaks were at 4.3 (020) and 2.5 Å (006).

PE compounds

The XRD studies of these compounds showed no changes in the diffraction patterns of the natural MMT clay (Cloisite Na^+) and organically treated MMT clay (Cloisite 20A) in the PE polymer matrix [Fig. 2(a)]. The *d*-spacing peaks of both clays were not shifted to lower

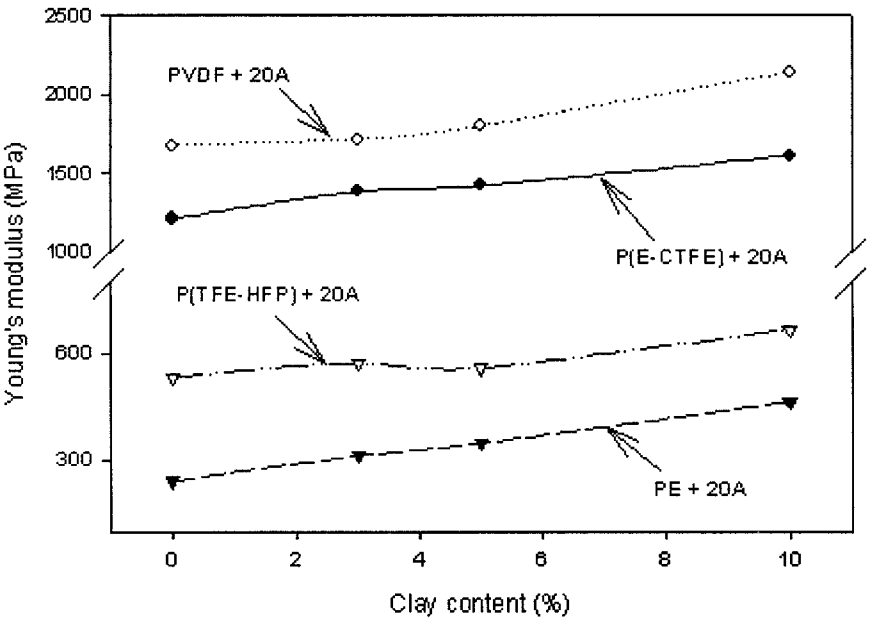

Figure 3 Young's modulus of PVDF, P(E-CTFE), P(TFE-HFP), PE, and Cloisite 20A compounds.

2θ angles. PE crystallized into the Bunn orthorhombic crystal structure and exhibited XRD peaks associated with its crystalline arrangement.

The TEM photomicrographs showed agglomerates of organically treated MMT clay (Cloisite 20A) in the PE polymer matrix. This suggested that PE polymer chains did not separate clay layers.

Young's modulus of the PE/20A compounds increased with the clay content (Fig. 3). PE/20A (3%) and PE/20A (5%) showed 30 and 44% increases, respectively. PE/20A (10%) showed a 93% growth of the modulus. The tensile strength of the PE/20A compounds was reduced as the clay content increased (Fig. 4). The elongation at break of the PE/20A compounds also decreased.

P(E-CTFE) compounds

The XRD studies of these compounds showed no changes in the diffraction patterns of the natural MMT clay (Cloisite Na^+) and organically treated MMT clay (Cloisite 20A) in the P(E-CTFE) polymer matrix. The

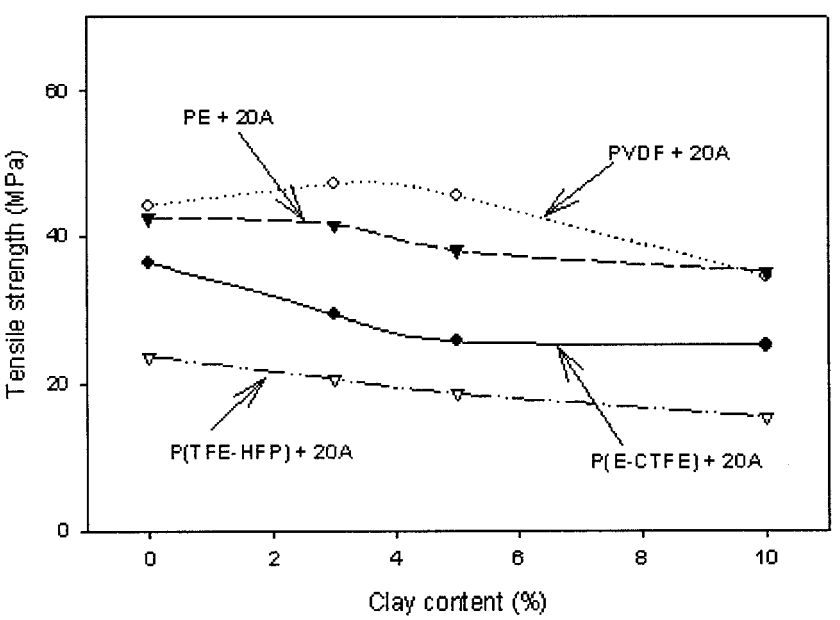

Figure 4 Tensile strength of PVDF, P(E-CTFE), P(TFE-HFP), PE, and Cloisite 20A compounds.

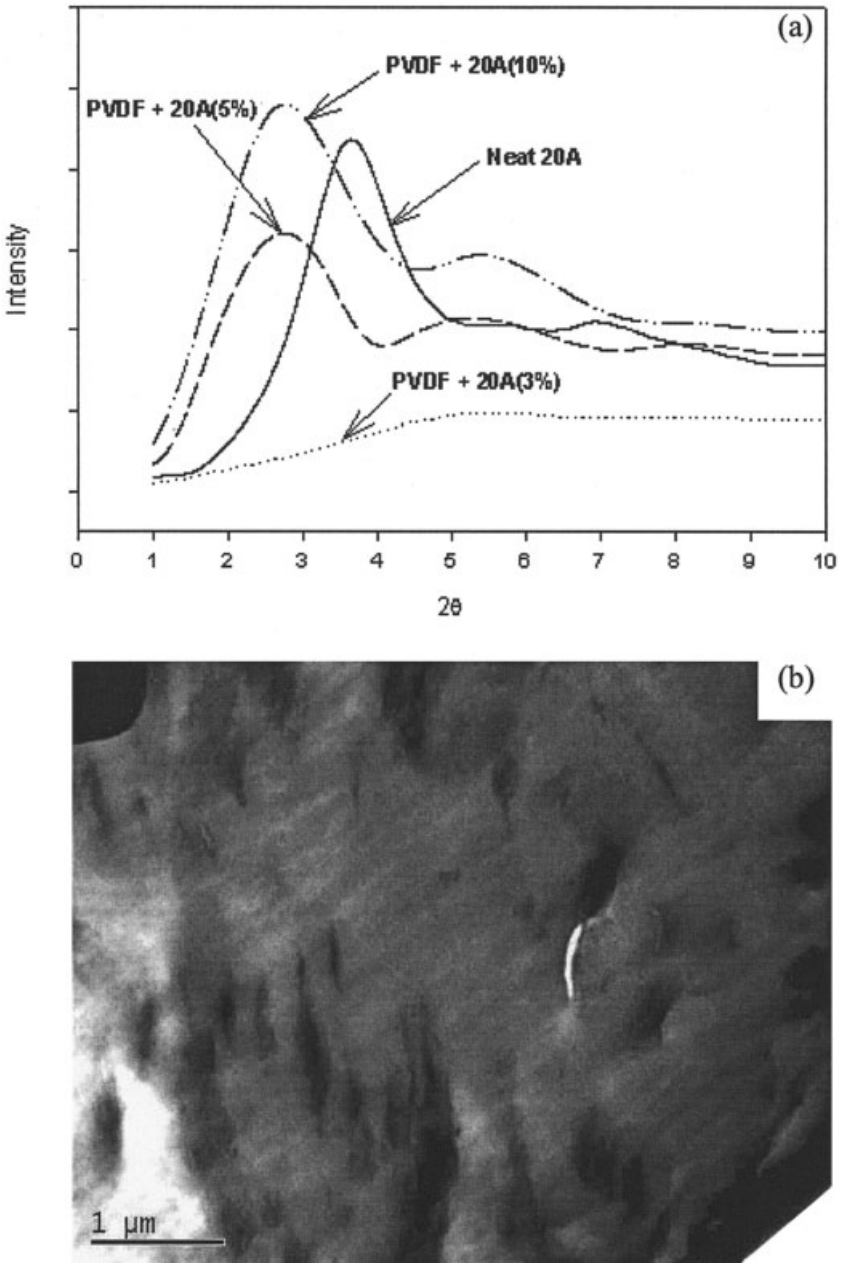

Figure 5 (a) XRD patterns and (b) TEM image of PVDF/20A compounds.

d-spacing peaks of the two clays were not shifted to lower 2θ angles.

The TEM photomicrographs showed agglomerates of organically treated MMT clay (Cloisite 20A) in the P(E-CTFE) polymer matrix [Fig. 2(b)]. They suggested that the clay layers were not separated by P(E-CTFE) polymer chains.

Young's modulus of the P(E-CTFE)/20A compounds increased with the clay content (Fig. 3). P(E-CTFE)/20A (3%) and P(E-CTFE)/20A (5%) showed 14 and 17% increases, respectively. P(E-CTFE)/20A (10%) showed a 32% growth of the modulus. The tensile strength of the P(E-CTFE)/20A compounds decreased as the clay content increased (Fig. 4). The tensile strength of P(E-CTFE)/20A (3%) decreased 19%. P(E-CTFE)/20A (5%) and P(E-CTFE)/20A (10%) exhibited 29 and 31% reductions, respectively. The elongation at break of the P(E-CTFE)/20A compounds also decreased.

PVDF compounds

PVDF is a crystalline thermoplastic and exhibits different peaks associated with its crystal structure. These are in the range of 17.2–19.9°.

No change in the X-ray data was observed in the compounds of PVDF and the natural MMT clay

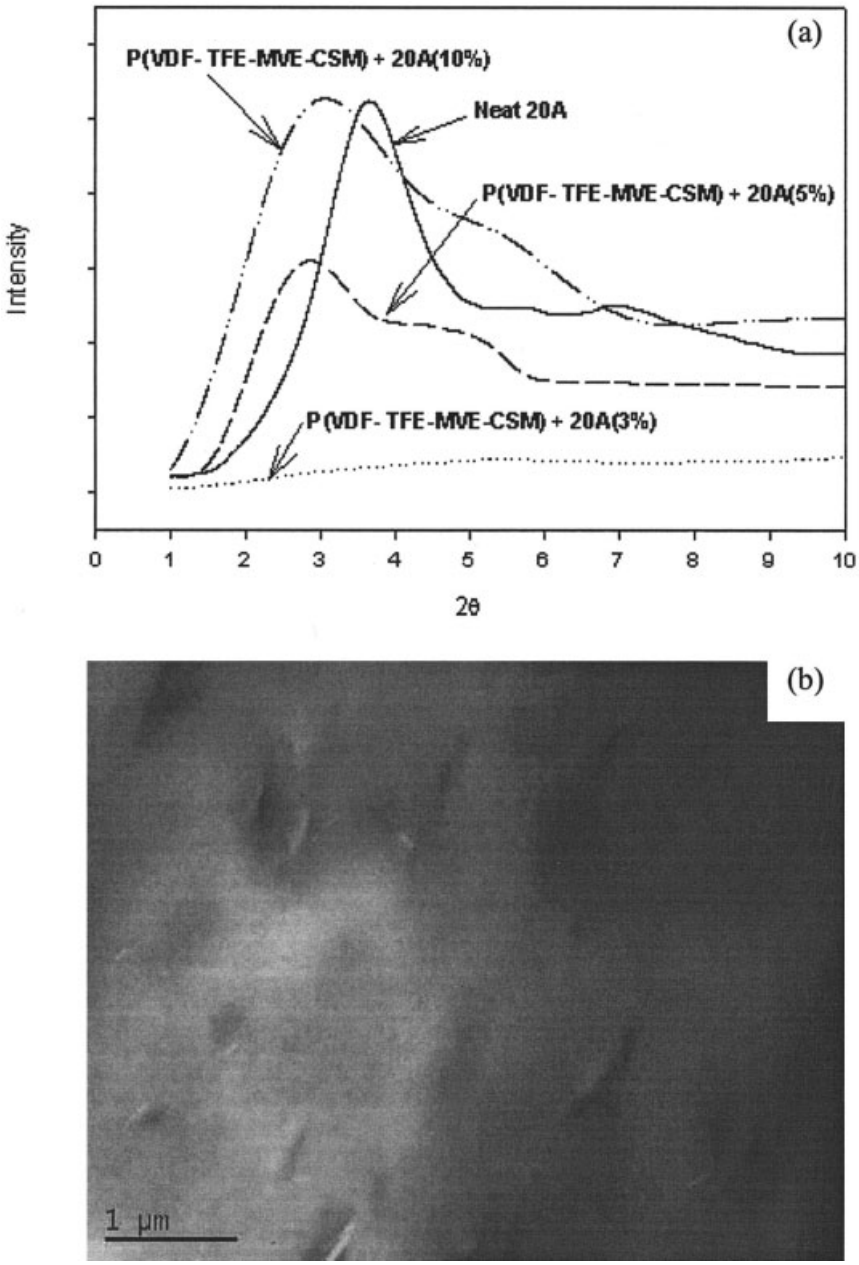

Figure 6 (a) XRD patterns and (b) TEM image of P(VDF-TFE-MVE-CSM)/20A compounds.

(Cloisite Na^+). Like PE, they exhibited a sum of the polymer and clay peaks.

For the organically modified clay (Cloisite 20A), Figure 5(a) shows the XRD results for the PVDF/20A compounds. PVDF containing 3% 20A did not show any *d*-spacing peaks below $2\theta = 10°$. The Cloisite 20A clay peaks in PVDF/20A (5%) and PVDF/20A (10%) were shifted to lower angles at $2\theta = 2.75°$ (the equivalent *d*-spacing was 32 Å).

The TEM image of a PVDF/20A compound showed dispersion of the clay layers [Fig. 5(b)]. It suggested that the PVDF polymer separated clay silicate layers.

Young's modulus of the PVDF/20A compounds was slightly enhanced with increasing clay content (Fig. 3). PVDF/20A (10%) had a 28% higher modulus than pure PVDF. Increasing the clay content enhanced the tensile strength of PVDF/20A compounds (Fig. 4). The tensile strength of PVDF/20A (3%) and PVDF/20A (5%) increased 7 and 3%, respectively, over that of pure PVDF. However, PVDF/20A (10%) exhibited a 22% reduction in the tensile strength. The elongation at break of the PVDF/20A compounds decreased.

P(VDF-TFE-MVE-CSM) compounds

The natural MMT clay (Cloisite Na^+) layers did not show changes in the *d*-spacing in the P(VDF-TFE-MVE-CSM) compounds.

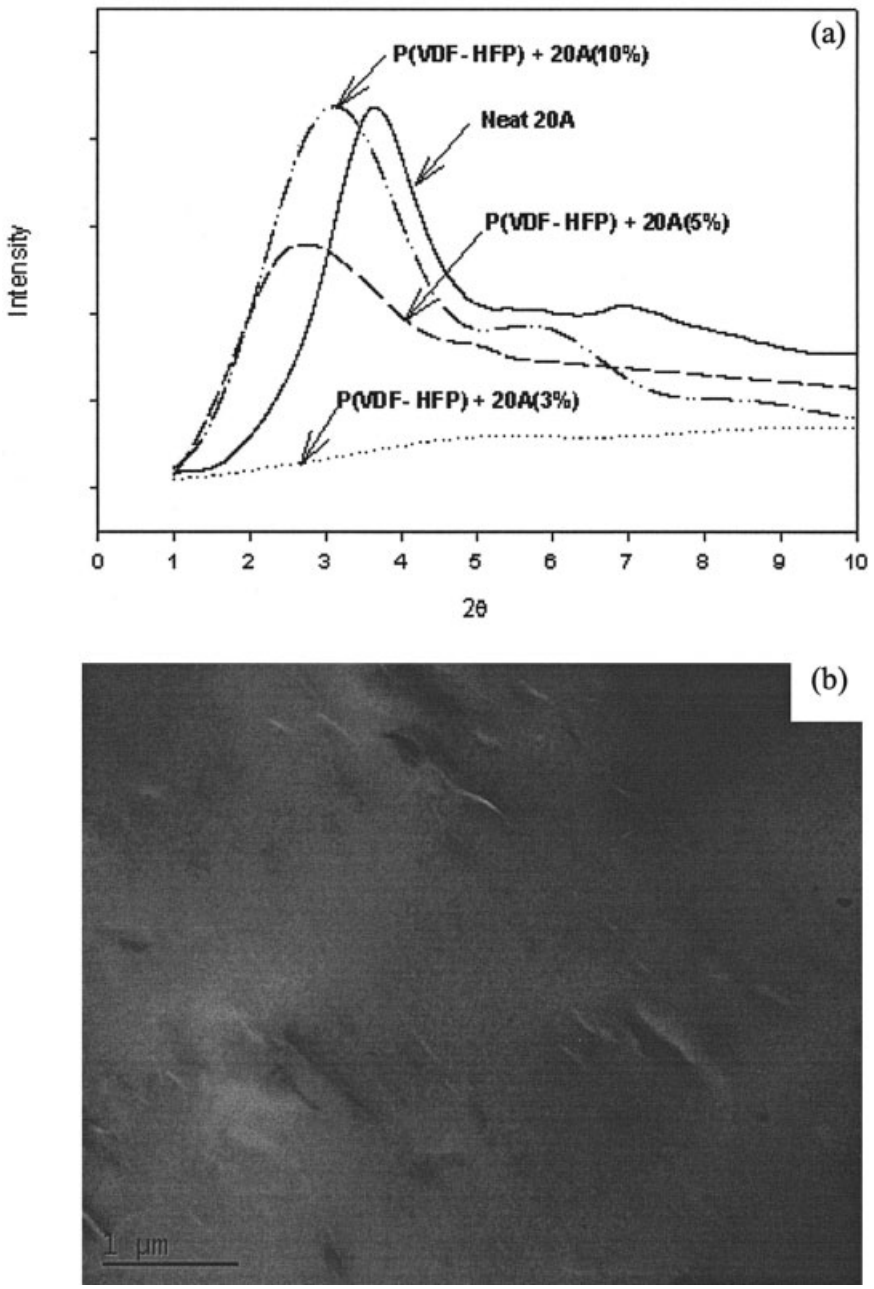

Figure 7 (a) XRD patterns and (b) TEM image of P(VDF-HFP)/20A compounds.

The clay peak was not observed in P(VDF-TFE-MVE-CSM)/20A (3%). P(VDF-TFE-MVE-CSM)/20A (5%) and P(VDF-TFE-MVE-CSM)/20A (10%) exhibited silicate layer clay peaks at $2\theta = 2.7°$ and $2\theta = 3.05°$, respectively, which corresponded to *d*-spacings of 32.7 and 29 Å [Fig. 6(a)]. This can be compared to 24.2 Å for the neat clay.

A TEM photomicrograph of a P(VDF-TFE-MVE-CSM)/20A compound suggested that P(VDF-TFE-MVE-CSM) polymer chains separated the silicate layers of MMT clay modified with Cloisite 20A [Fig. 6(b)].

P(VDF-HFP) compounds

There was no change in the clay WAXS pattern of natural MMT clay (Cloisite Na^+) in the P(VDF-HFP) polymer matrix.

A TEM image and XRD patterns, however, indicated some breakup of the clay platelets of MMT clay modified with Cloisite 20A in the P(VDF-HFP) polymer matrix.

The clay peak of organically treated 20A of a P(VDF-HFP)/20A (3%) compound was not observed [Fig. 7(a)]. P(VDF-HFP)/20A (5%) and P(VDF-HFP)/20A

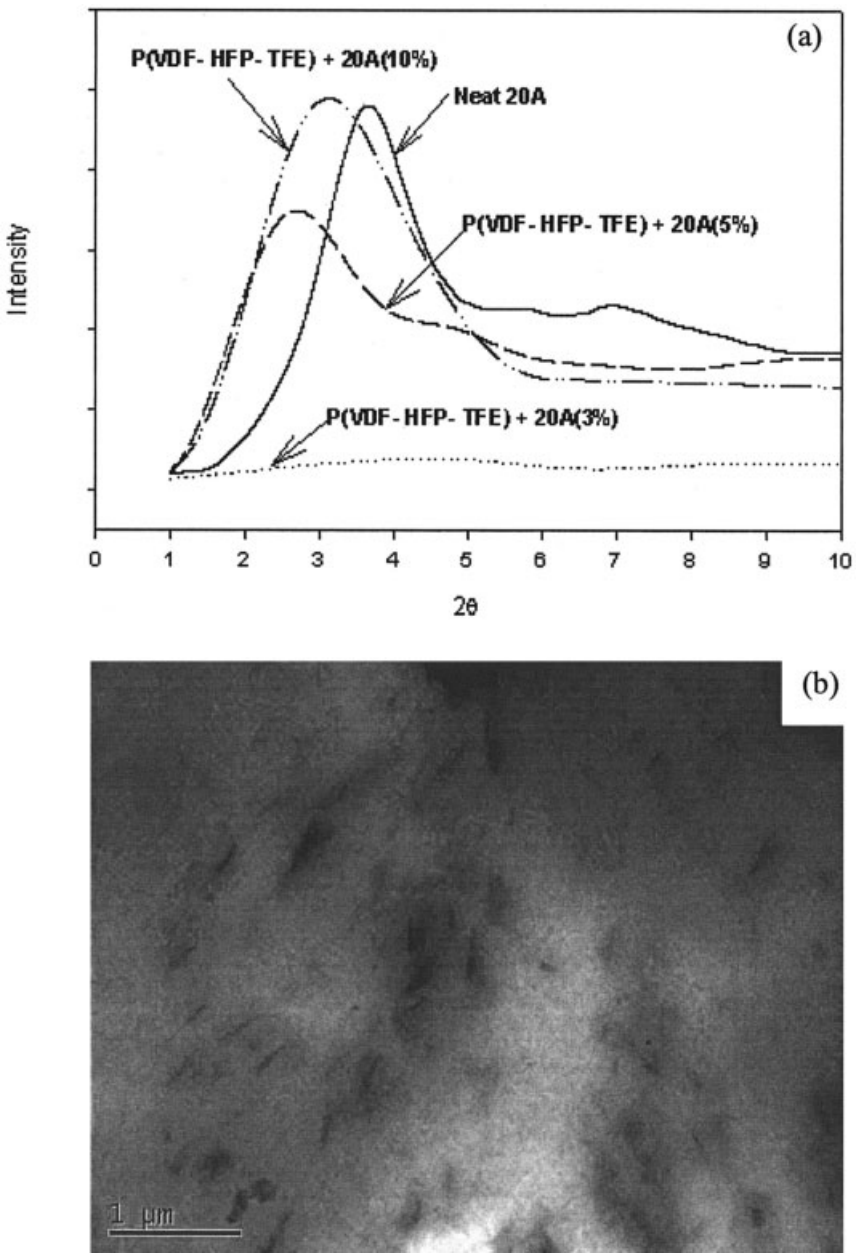

Figure 8 (a) XRD patterns and (b) TEM image of P(VDF-HFP-TFE)/20A compounds.

(10%) had their clay peaks at $2\theta = 2.7°$ and $2\theta = 3.1°$, respectively, which are equivalent to *d*-spacings of 32.7 and 28.5 Å. These values can be compared to 24.2 Å for the neat clay.

The TEM photomicrograph in Figure 7(b) suggests clay particle breakup on the nanometer scale. This TEM image of P(VDF-HFP)/20A shows the separation of clay layers.

P(VDF-HFP-TFE) compounds

There was no shift in the clay XRD peaks of natural MMT clay (Cloisite Na^+) layers in the P(VDF-HFP-TFE) polymer.

Figure 8(a) shows the XRD test results for the P(VDF-HFP-TFE)/20A compounds. The clay peaks did not appear for P(VDF-HFP-TFE)/20A (3%). The silicate layer clay peaks for P(VDF-HFP-TFE)/20A (5%) and P(VDF-HFP-TFE)/20A (10%) were shifted to lower angles at $2\theta = 2.85°$ and $2\theta = 3.05°$, respectively, which correspond to 31 and 29 Å. These lower angle clay peaks represented the expansion of the basal spacing of clay layers in the P(VDF-HFP-TFE)/20A compounds.

A TEM photomicrograph suggests the clay separation of the P(VDF-HFP-TFE)/20A compounds [Fig. 8(b)]. P(VDF-HFP-TFE) polymer chains intercalated clay particles. The penetration of P(VDF-HFP-TFE)

polymer chains into clay layers can be surmised from the TEM results and XRD analysis.

P(TFE-HFP) compounds

The natural MMT (Cloisite Na^+) and organically treated MMT clay (Cloisite 20A) layers in the P(TFE-HFP) did not show the *d*-spacing increasing in XRD. The basal spacing peaks of the P(TFE-HFP)/20A compounds were shifted to a larger angle, $2\theta = 5.55°$, which corresponds to a *d*-spacing of 15.9 Å.

A TEM photomicrograph of a P(TFE-HFP)/20A compound showed agglomerates of organically treated MMT clay (Cloisite 20A) and suggested no separation of the clay layers.

P(TFE-HFP)/20A compounds showed higher modulus than pure P(TFE-HFP) (Fig. 3). P(TFE-HFP)/20A (10%) showed a 25% elevated modulus. Increasing the clay content reduced the tensile strength of the P(TFE-HFP)/20A compounds (Fig. 4). The tensile strength of P(TFE-HFP)/20A (3%) decreased 13% from that of pure P(TFE-HFP). P(TFE-HFP)/20A (5%) and P(TFE-HFP)/20A (10%) showed 22 and 35% reductions, respectively, in their tensile strength. The elongation at break of the P(TFE-HFP)/20A compounds decreased with the clay content.

INTERPRETATION

Mechanism

The observations of this study and our previous study[21] indicate that polyolefins do not form nanocomposites by melt mixing. Polystyrene (PS) also has been found to have problems in forming nanocomposites. We have found that homopolymers containing both fluorine and chlorine intercalate to form nanocomposites. This is notably the case with polymers containing the following structural units:

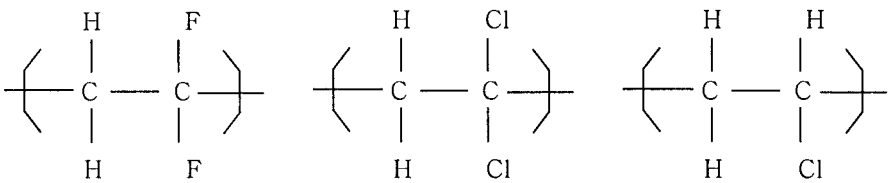

More disordered copolymers, such as chlorinated PE and chlorinated PVC, also form nanocomposites with melt mixing. Nanocomposites can be formed from fluorinated copolymers as long as they contain vinylidene fluoride (VDF), but not from copolymers without VDF.

The previous discussion seems to suggest that dipoles in the polymer backbone or the backbone and side groups lead to the formation of nanocomposites. Similar conclusions were expressed by Blumstein,[8] as early as 1965, about polar organic liquids (monomers) swelling natural MMT.

The readily measurable material property that is most closely related to dipoles is the dielectric constant (ϵ/ϵ_0 or ϵ). For materials without dipoles, such as aliphatic hydrocarbons, ϵ is given by the Clausius–Mosotti equation:[31]

$$\frac{\varepsilon - 1}{\varepsilon + 2} = \frac{N\alpha}{3} \tag{1}$$

where α is the molecular polarizability and N is the molecular density. For materials with dipoles, the dielectric properties have been variously modeled by Debye,[32,33] Onsager,[34] and Kirkwood.[35,36] They all reported that the ϵ values increased with dipole moments (μ). Debye's formulation is

$$\frac{\varepsilon - 1}{\varepsilon + 2} = \frac{N}{3}\left[\alpha + \frac{\mu^2}{3\kappa_B T}\right] \tag{2}$$

The idea of a polymer having a μ value seems favorable to it penetrating silicate layers. This suggests that the formation of polymer nanocomposites should be favored by high ϵ values. This relationship is explored in Table II. It seems that an ϵ value greater than 3.1 or a μ value greater than 0.5 D ensures the formation of a nanocomposite by melt mixing.

P(TFE-HFP)/20A degradability

For P(TFE-HFP), the polymer backbone chains are surrounded completely by fluorine atoms. It has a

TABLE II
ϵ and μ Values of the Polymers[37–39]

Material	ϵ	μ (D)	Melt-intercalation nanocomposite
P(TFE-HFP)	2.1	0.27	No?
PP	2.25	Not applicable	No
PE	2.3	0.07	No
P(E-CTFE)	2.6	0.41	No
PS	2.8	0.42	No
PVC	3.4	0.52	Yes
CR	4.9	0.91	Yes
PVDC	4.67	0.70	Yes
P(VDF-HFP-TFE)[a]	5.19	0.92	Yes
P(VDF-TFE-MVE-CSM)	7.2	—	Yes
P(VDF-HFP)	7.6	—	Yes
PVDF	8.4	0.89	Yes

[a] Fluoroplastic.

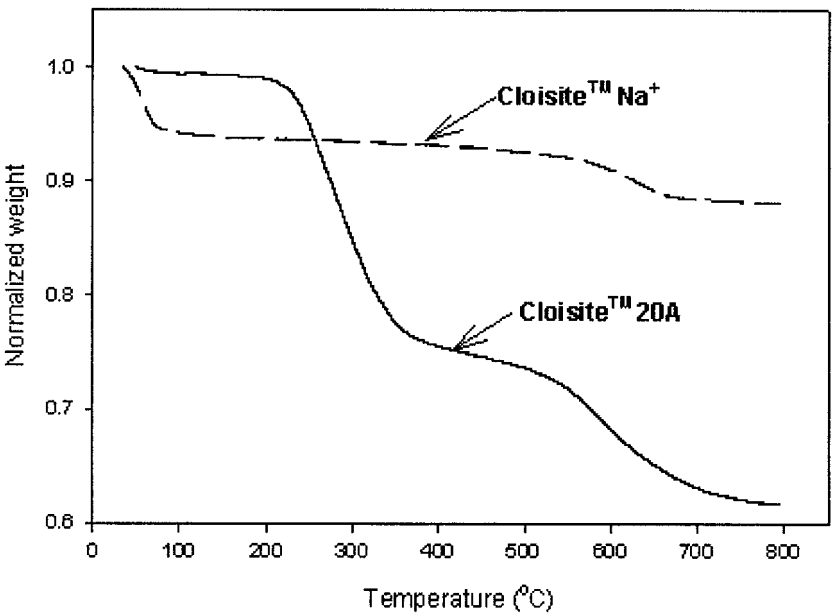

Figure 9 Thermogravimetric analysis of Cloisite 20A and Na^+ MMT clays.

very low value of ϵ. The P(TFE-HFP)/20A compounds did not show clay separation in this study. However, the organic modifiers in Cloisite 20A could be thermally degraded at a high mixing temperature (264°C; Fig. 9), as described by Xie et al.[40] This thermal degradation of organic modifiers might cause the *d*-spacing to decrease from 24.2 to 15.9 Å; this can be compared to other explanations of *d*-spacing reductions.[41]

CONCLUSIONS

In PVDF and the fluoroelastomers P(VDF-HFP), P(VDF-TFE-CSM), and P(VDF-HFP-TFE), organically treated MMT (Cloisite 20A) was able to intercalate the silicate layers well. There was no intercalation of clay layers in P(E-CTFE) and PE. The polarity of the VDF-containing fluorinated polymers and the organophilicity of modified MMT clay could be the reasons for the formation of nanocomposites. XRD and TEM characterizations proved the intercalation of clay platelets. The mechanical properties of the PVDF/20A nanocomposites were enhanced in comparison with those of pristine fluoropolymers. The ϵ values of the chlorinated and fluorinated polymers were related to μ, which contributed to the melt intercalation to form polymer–clay nanocomposites.

References

1. Plunkett, R. J. (to E. I. Du Pont de Nemours and Co.). U.S. Pat. 2,230,654 (1941).
2. Scheirs, J. Modern Fluoropolymers: High Performance Polymers for Diverse Applications; Wiley: New York, 1997.
3. Lee, E. S. Ph.D. Dissertation, University of Akron, 1997.
4. (a) Hofmann, U.; Endell, K.; Wilm, D. Z Kristallogr Miner Petrogr Abt A 1993, 86, 340; (b) Hofmann, U.; Endell, K.; Wilm, D. Angew Chem 1934, 47, 539.
5. Bradley, W. F. J Am Chem Soc 1945, 67, 975.
6. Norrish, K. Discuss Faraday Soc 1954, 18, 120.
7. Weiss, A. Angew Chem Int Ed 1963, 2, 134.
8. Blumstein, A. J Polym Sci Part A: Gen Pap 1965, 3, 2653.
9. Solomon, D. H.; Loft, B. C. J Appl Polym Sci 1968, 12, 1253.
10. Fukushima, Y.; Okada, A.; Kawasumi, M.; Kurauchi, T.; Kamigaito, O. Clay Mater 1988, 23, 27.
11. Usuki, A.; Kojima, Y.; Kawasumi, M.; Okada, A.; Fukushima, Y.; Kurauchi, T.; Kamigaito, O. J Mater Res 1993, 8, 1179.
12. Kojima, Y.; Usuki, A.; Kawasumi, M.; Okada, A.; Kurauchi, T.; Kamigaito, O. J Polym Sci Part A: Polym Chem 1993, 31, 983.
13. Usuki, A.; Kawasumi, M.; Kojima, Y.; Okada, A.; Kurauchi, T.; Kamigaito, O. J Mater Res 1993, 8, 1174.
14. Kojima, Y.; Usuki, A.; Kawasumi, M.; Okada, A.; Kurauchi, T.; Kamigaito, O. J Polym Sci Part A: Polym Chem 1993, 31, 1755.
15. Kojima, Y.; Usuki, A.; Kawasumi, M.; Okada, A.; Kurauchi, T.; Kamigaito, O.; Kaji, K. J Polym Sci Part B: Polym Phys 1994, 32, 625.
16. Kojima, Y.; Usuki, A.; Kawasumi, M.; Okada, A.; Fukushima, Y.; Kurauchi, T.; Kamigaito, O. J Mater Res 1993, 8, 1185.
17. Liu, X.; Wu, Q. Macromol Mater Eng 2002, 287, 180.
18. Riva; Zanetti, M.; Braglia, M.; Camino, G.; Falqui, L. Polym Degrad Stab 2002, 77, 299.
19. Wang, D.; Parlow, D.; Yao, Q.; Wilkie, C. A. J Vinyl Additive Tech 2001, 7, 203.
20. Hinojosa-Falcon, L. A.; Goettler, L. A. Soc Plast Eng Annu Tech Conf Tech Pap 2002, 2, 1509.
21. Kim, Y.; White, J. L. J Appl Polym Sci, to appear.
22. Kawasumi, M.; Hasegawa, N.; Kato, M.; Usuki, A.; Okada, A. Macromolecules 1997, 30, 6333.
23. Usuki, A.; Kato, M.; Okada, A.; Karauchi, T. J Appl Polym Sci 1997, 63, 137.
24. Kato, M.; Usuki, A.; Okada, A. J Appl Polym Sci 1997, 66, 1781.

25. Hasegawa, N.; Kawasumi, M.; Kato, M.; Usuki, A.; Okada, A. J Appl Polym Sci 1998, 67, 87.
26. Hasegawa, N.; Okamoto, H.; Kato, M.; Usuki, A. J Appl Polym Sci 2000, 78, 1918.
27. Lim, Y. T.; Park, O. O. Rheol Acta 2001, 40, 220.
28. Priya, L.; Jog, J. P. J Polym Sci Part B: Polym Phys 2002, 40, 1682.
29. Badesha, S. S.; Henry, A. W.; Maliborski, J. B.; Eddy, C. O. U.S. Pat. 5,840,796 (1998).
30. Michalczyk, M. J.; Sharp, K. G.; Stewart, C. W. U.S. Pat. 5,726,247 (1998)
31. Sommerfeld; Electrodynamics; Academic: New York, 1948.
32. Debye, P. Phys Z 1912, 13, 97.
33. Debye, P. Polar Molecules; Dover: New York, 1929.
34. Onsager, L. J Am Chem Soc 1936, 58, 1486.
35. Kirkwood, J. G. J Chem Phys 1939, 7, 911.
36. Kirkwood, J. G. Trans Faraday Soc A 1946, 42, 7.
37. Drobny, J. G. Technology of Fluoropolymers; CRC: Boca Raton, FL, 2001.
38. Polymer Handbook, 2nd ed.; Brandrup, J., Immergut, E. H., Eds.; Wiley: New York, 1975.
39. Encyclopedia of Chemical Technology, 4th ed.; Kroschwitz, J. I., Ed.; Wiley: New York, 1998.
40. Xie, W.; Gao, Z.; Pan, W. P.; Hunter, D.; Singh, A.; Vaia, R. Chem Mater 2001, 13, 2979.
41. Gilman, J. W.; Awad, W. H.; Davis, R. D.; Shields, J.; Harris, R. H., Jr.; Davis, C.; Morgan, A. B.; Sutto, T. E.; Callahan, J.; Trulove, P. C.; DeLong, H. C. Chem Mater 2002, 14, 3776.